PHYSICAL REVIEW B **93**, 014401 (2016)

Engineering closed optical transitions in rare-earth ion crystals

John G. Bartholomew,* Rose L. Ahlefeldt,† and Matthew J. Sellars
Centre for Quantum Computation and Communication Technology, Laser Physics Centre, The Australian National University, Canberra, Australian Capital Territory 2601, Australia

(Received 23 July 2015; revised manuscript received 23 November 2015; published 4 January 2016)

We propose a protocol to preserve the spin state of rare-earth ions when they are optically cycled. This technique uses large magnetic fields to increase the probability of an optically excited ion returning to its initial spin state. This Zeeman enhanced cyclicity is shown to be applicable to non-Kramers ions in various crystals irrespective of the site symmetry. The specific example of Pr^{3+}:Y_2SiO_5 is investigated to demonstrate that the protocol can create closed optical transitions even where the point group symmetry of the site is C_1. In this example, the predicted cyclicity exceeds 10^4. This high level of cyclicity extends the usefulness of rare-earth ion crystals for applications in quantum and classical information processing. We explore the use of this technique to enable single-ion, spin-state optical readout and the creation of ensemble-based spectral features that are robust against optical cycling.

DOI: 10.1103/PhysRevB.93.014401

I. INTRODUCTION

Like trapped gases, solid-state rare-earth ion materials can possess extremely narrow optical resonances, with homogeneous linewidths as narrow as 50 Hz [1]. Furthermore, ground-state hyperfine level lifetimes have been measured to be as long as 23 days [2] and the coherence times for transitions between such levels have been extended beyond six hours [3]. Rare-earth ion crystals are also inherently stable because the crystal lattice prohibits spatial diffusion, while spectral diffusion is limited by the insensitivity of the ions to electric and magnetic perturbations.

The narrow and stable optical and spin transitions that are found in systems such as trapped vapors and rare-earth crystals can be manipulated precisely with electromagnetic fields. The pairing of precise control with the high degree of isolation from environmental perturbations observed in both these systems provides opportunities for many applications. For rare-earth ion crystals, such applications include classical data storage [4] and processing [5], frequency references [6], quantum memories [7,8], and nonclassical light sources [9].

Although trapped vapor systems and rare-earth ion crystals have many similarities in their properties and potential applications, there are several important differences. This paper focuses on one such difference: the existence of closed optical transitions. A closed optical transition is formed when a quantum system can be repetitively cycled within a chosen set of energy levels without decaying to a state outside this chosen set [see Fig. 1(a)]. Being able to repetitively cycle within closed transitions is important for processes such as laser cooling and high-fidelity single-ion quantum-state readout [10,11].

Closed transitions exist in trapped gases because electronic and spin selection rules allow transitions within the chosen set of states whereas other transitions are forbidden. As a result, ensembles or single emitters can be optically cycled within the closed transition with high efficiency or alternatively shelved to an auxiliary level outside the chosen set.

Closed optical transitions seldom occur between the $4f^N$ levels of rare-earth ions in a solid-state matrix [see Fig. 1(b)]. The $4f^N$ levels in a solid are strong admixtures of the levels that exist for a free ion. This is a consequence of the crystal field interaction, which admixes states of opposite parity, and different electron spin angular momentum J. As a result, quantum selection rules do not define allowed or forbidden transitions between $4f^N$ levels but rather a myriad of weakly allowed transitions.

In sites without perfect axial symmetry, the inability to form closed transitions also extends to sets of hyperfine spin states. This is because the asymmetry of the electric field gradient acting on the ion nucleus creates hyperfine nuclear spin states that are admixtures of pure I_z states. Because the spin-state admixtures differ for different crystal field levels, the optical transition can induce a change in the hyperfine state. While this process allows spin-state preparation and population shelving using optical pumping, it also prevents the formation of closed optical transitions defined by sets of spin states.

In this paper, we show that it is possible to control the hyperfine state admixtures with magnetic fields to create closed optical transitions. By applying large magnetic fields along a specific direction, the resultant hyperfine eigenstates of the ground- and excited-state crystal field levels coincide. This effectively creates allowed and forbidden transitions. This Zeeman enhanced cyclicity (ZEC) allows closed optical transitions to exist that are defined by the hyperfine spin states. This means that an ion's initial hyperfine state can be preserved upon repeated optical cycling, something that has not previously been possible in rare-earth ion crystals.

The paper focuses on non-Kramers ions in noncentrosymmetric crystalline sites where the ground and excited crystal field levels are electronic singlets: all sites for Eu^{3+}, and sites with less than threefold-rotational symmetry for Pr^{3+}, Tb^{3+}, Ho^{3+}, and Tm^{3+} [12].

We divide the paper into six further sections. Section II presents the foundations of the proposed technique and explains why it is possible for closed optical transitions to be

*Current address: PSL Research University, Chimie ParisTech CNRS, Institut de Recherche de Chimie Paris, 75005 Paris, France; john.g.bartholomew@gmail.com
†Current address: Department of Physics, Montana State University, Bozeman, MT 59717.

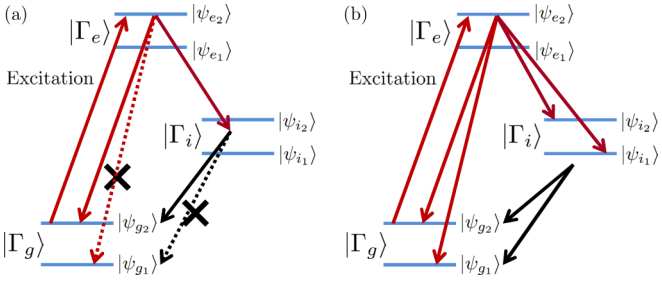

FIG. 1. The difference between the relaxation paths for a closed optical transition (a) and a general $4f^N \leftrightarrow 4f^N$ transition in rare-earth ion crystals (b). $|\Gamma_g\rangle$ and $|\Gamma_e\rangle$ represent the ground- and excited-state crystal field levels, and $|\Gamma_i\rangle$ represents an intermediate crystal field level. The $|\psi\rangle$ represent the hyperfine states of the respective electronic levels. The red arrows represent photon interactions whereas the black arrows represent phonon decay. In (a), relaxation from $|\Gamma_e\rangle|\psi_{e_2}\rangle$ can only terminate in $|\Gamma_g\rangle|\psi_{g2}\rangle$ and hence, the transition is closed. In (b) relaxation can terminate in any of the ground-state hyperfine levels making a closed transition impossible.

formed from sets of hyperfine spin states. In Sec. III, the ZEC concept is developed into equations that describe the necessary field directions to create cyclic transitions in the high-field limit. In Sec. IV, we examine the form of the solutions for ZEC field directions in sites with axial, orthorhombic, and C_2 point group symmetry. This discussion illustrates that the complexity of the solutions increases as the site symmetry decreases towards C_1 point group symmetry. To show the ZEC field solutions for a C_1 site, specific calculations are performed for Pr^{3+}:Y_2SiO_5 in Sec. V. These calculations include a quantitative analysis of the theoretically achievable cyclicity and the effect of field misalignment. Section VI describes two applications of ZEC. The first application is direct single rare-earth ion qubit readout for quantum information processing. The second is the engineering of write-once, read-many (WORM) spectral features, which have applications in both classical and quantum memory protocols. The paper then concludes with a brief discussion of the experimental considerations that will be important to realize ZEC in Sec. VII.

II. FORMING CLOSED OPTICAL TRANSITIONS USING HYPERFINE SPIN STATES

In this section, we explain why closed optical transitions can be formed by manipulating the hyperfine states with ZEC. An important part of this explanation is the ability to separate the ion's wave function into electronic and nuclear components, which is justified in Sec. II A. In Sec. II B, we show that the wave-function separation allows for closed optical transitions to be defined using the hyperfine spin states. Finally, in Sec. II C we present a condition on the ion's optical relaxation for this simple method to be effective in closing optical transitions.

A. Separating the wave function

The $4f^N$ energy levels in rare-earth ion crystals are defined by the Hamiltonian

$$\widehat{H} = \widehat{H}_{\text{fi}} + \widehat{H}_{\text{cf}} + \widehat{H}_{\text{mh}}, \tag{1}$$

where $\widehat{H}_{\text{fi}}$ is the Hamiltonian for the free ion, $\widehat{H}_{\text{cf}}$ describes the crystal field interaction, and $\widehat{H}_{\text{mh}}$ is the magnetic hyperfine interaction [13,14].

For non-Kramers electronic singlets, the electronic states are completely defined by $\widehat{H}_{\text{fi}}$ and $\widehat{H}_{\text{cf}}$. The free-ion and crystal field interactions are several orders of magnitude larger than the magnetic hyperfine interactions. This means $\widehat{H}_{\text{mh}}$, which governs the nuclear hyperfine states, can be treated as a perturbation to the electronic interactions. This allows the $4f^N$ wave functions to be separated into electronic and nuclear components

$$|g\rangle \approx |\Gamma_g\rangle|\psi_g\rangle, \quad |e\rangle \approx |\Gamma_e\rangle|\psi_e\rangle, \tag{2}$$

where the Γ_j and ψ_j represent the electronic and nuclear hyperfine components of the ground and excited states, respectively (see Fig. 1).

Given that the wave function is separable, the transition probability from $|e\rangle$ to $|g\rangle$ can now be examined through the application of an operator $\widehat{\boldsymbol{O}}$ that governs the optical transition. For example, $\widehat{\boldsymbol{O}} = \widehat{\boldsymbol{\mu}}\cdot\boldsymbol{E}$ for electric dipole transitions, and similar expressions can be written for magnetic dipole transitions, electric quadrupole transitions, and other higher-order operators:

$$|\langle e|\widehat{\boldsymbol{O}}|g\rangle|^2 \approx |\langle\Gamma_e|\widehat{\boldsymbol{O}}|\Gamma_g\rangle|^2|\langle\psi_e|\psi_g\rangle|^2. \tag{3}$$

The first term on the right-hand side of Eq. (3) governs the overall dynamics of the optical transition, such as the branching ratio and oscillator strength, and is equal for any of the states in the hyperfine manifold. The relative spin transition probabilities are given by the nuclear magnetic component. This term is simply the overlap between the ground- and excited-state spin wave functions and is the focus of this paper.

B. Definition of cyclicity

The previous section showed that the optical transition probability between two $4f^N$ levels is proportional to the overlap of the excited-state and ground-state hyperfine wave functions. Closed optical transitions can be achieved if this term is engineered such that

$$|\langle\psi_{e_j}|\psi_{g_k}\rangle|^2 = \begin{cases} 0 & \text{if } j \neq k, \\ 1 & \text{if } j = k, \end{cases} \tag{4}$$

where j and k are labels based on the energy ordering of the hyperfine states. Equation (4) defines a cyclic transition.

This paper focuses on manipulating the $\langle\psi_e|\psi_g\rangle$ term with applied magnetic fields to approach the condition for cyclicity defined in Eq. (4). It is interesting to note that the concept of altering the zero-field transition probabilities of non-Kramers rare-earth ions in crystals has been explored previously in the context of creating efficient Λ transitions in Tm^{3+}:YAG[15,16] and Pr^{3+}:$YLiF_4$ [17]. This is, in many ways, precisely the opposite goal of this paper. In Refs. [15,17] the aim was to create a Λ transition in sites with high point group symmetries (D_2 for Tm^{3+}:YAG and S_4 for Pr^{3+}:$YLiF_4$) for which the two branches of the transition had equal probabilities $|\langle\psi_e|\psi_g\rangle|^2$. In this paper, we investigate cyclicity, a more stringent condition, with a method applicable to all sites with noncentrosymmetric point group symmetries.

C. A condition for creating cyclicity via manipulation of $\langle\psi_e|\psi_g\rangle$

To close an optical transition, there are four stages that need to be considered to justify the ZEC approach: excitation, the duration in $|e\rangle$, relaxation, and the duration in $|g\rangle$ before reexcitation. We consider the evolution of the $\langle\psi_e|\psi_g\rangle$ term during all four of these stages. The relaxation process is particularly important because it involves intermediate crystal field levels possessing distinct hyperfine interactions. We present a requirement on the relaxation process for cyclicity to be achieved through this simple criteria.

The direct excitation of the transition $|\Gamma_g\rangle|\psi_g\rangle \rightarrow |\Gamma_e\rangle|\psi_e\rangle$ is controlled via the applied laser frequency. Because of the O(kHz) homogeneous linewidths of rare-earth $4f^N \leftrightarrow 4f^N$ transitions in the materials of interest, the O(MHz) hyperfine level separations allow each level to be spectrally resolved. Although there is a finite probability of off-resonant excitation to another excited-state hyperfine level, it is assumed that the Rabi frequency can be sufficiently decreased to eliminate this effect.

The next consideration is whether there is any evolution of the ion's spin state when it resides in $|e\rangle$ after excitation or in $|g\rangle$ after relaxation. At low temperature, the hyperfine manifolds are sufficiently decoupled from the lattice to possess lifetimes as long as 100 s [18] to 20 days [2]. In comparison, the optical excited-state lifetime and the delay between excitation pulses are commonly of the order of milliseconds for most applications. Therefore, the hyperfine state of the ion is preserved during these stages of the cycling process.

The final consideration is the possible perturbation to the hyperfine structure during the relaxation process. It is necessary to consider two types of relaxation paths to the ground state: relaxation via the direct optical transition and relaxation through intermediate states. For a more detailed treatment of both these cases, the reader is directed to Appendix A.

In the case of a direct optical transition from $|\Gamma_e\rangle|\psi_e\rangle \rightarrow |\Gamma_g\rangle|\psi_{g_n}\rangle$, the hyperfine state of the ion is unaffected giving the obvious term for the transition probability: $|\langle\psi_e|\psi_{g_n}\rangle|^2$. However, the branching ratio for the direct optical transition is typically < 0.1 because of the numerous weakly allowed transitions that exist between electronic states in rare-earth ion crystals. Therefore, the dominant relaxation path is through intermediate levels.

We first consider an individual indirect pathway through one intermediate level as shown in Fig. 1(b). When the ion relaxes from $|\Gamma_e\rangle|\psi_e\rangle$ to the intermediate crystal field level $|\Gamma_i\rangle$, the hyperfine state $|\psi_e\rangle$ is initially unchanged. In general, $|\psi_e\rangle$ is not within the set of hyperfine eigenstates $|\psi_{i_m}\rangle$ of $|\Gamma_i\rangle$, which are defined by the spin Hamiltonian $\widehat{H}_i$:

$$\widehat{H}_i|\psi_{i_m}\rangle = E_{i_m}|\psi_{i_m}\rangle = \hbar\omega_m|\psi_{i_m}\rangle. \tag{5}$$

The state $|\psi_e\rangle$ can be represented as a superposition of the $|\psi_{i_m}\rangle$ in the form

$$|\psi_e\rangle = \sum_m c_{i_m}|\psi_{i_m}\rangle. \tag{6}$$

The ion will remain in $|\Gamma_i\rangle$ for a time τ governed by the lifetime of that state. During time τ, the superposition state of Eq. (6) will evolve. Each term in the superposition will accumulate a phase $e^{-i\omega_m\tau}$:

$$|\psi(\tau)\rangle = \sum_m e^{-i\omega_m\tau}c_{i_m}|\psi_{i_m}\rangle. \tag{7}$$

If $\tau \ll {\omega_m}^{-1}$ (for $m = 1, \ldots, 2I+1$), the accumulated phases $e^{-i\omega_m\tau} \approx 1$ and the initial state is preserved: $|\psi\rangle(\tau) = |\psi_e\rangle$. That is, a sufficiently rapid indirect transition from $|\Gamma_e\rangle|\psi_e\rangle$ to $|\Gamma_g\rangle|\psi_{g_n}\rangle$ through $|\Gamma_i\rangle$ can be considered to be a diabatic passage [19] with the transition probability given by $|\langle\psi_e|\psi_{g_n}\rangle|^2$.

The diabatic criterion can be extended to indirect transitions containing multiple intermediate states. This means that if the relaxation process through the intermediate levels is sufficiently rapid, cyclicity can be controlled by manipulation of the resonant state hyperfine levels.

There are many rare-earth ion materials for which the diabatic criterion is satisfied because there is an absence of metastable states. For example, the electronic structure of europium in crystalline environments makes it a good candidate for ZEC because all relaxation pathways should fulfill the diabatic condition. In general, the six intermediate LSJ manifolds between the ${}^5D_0$ excited state and ${}^7F_0$ ground state all possess small energy separations compared to the crystal's maximum phonon energy [20]. As a result, relaxation is dominated by rapid [O(ns)] decay mediated by multiphonon transitions [21].

If metastable electronic states exist (τ is comparable to ${\omega_m}^{-1}$), then further criteria need to be met for cyclicity to be controlled by manipulating $\langle\psi_e|\psi_{g_n}\rangle$. To complete this section, we provide a brief statement regarding an alternate criterion, which will be discussed further in Sec. VII A. In the analysis above we have considered the most general case where $|\psi_e\rangle$ is not an eigenstate of $\widehat{H}_i$. In the more specific case where $|\psi_e\rangle$ is an eigenstate of $\widehat{H}_i$ ($|\psi_e\rangle = |\psi_{i_m}\rangle$) for all $|\Gamma_i\rangle$, no evolution of the hyperfine state will occur during relaxation. This is because the phase term $e^{-i\omega_m\tau}$ does not change the state mixing irrespective of the lifetimes τ of the intermediate levels. In Sec. IV, we show that this criterion can be satisfied by using the ZEC technique in sites that possess a proper rotation axis of symmetry.

III. ENHANCING CYCLICITY IN NON-KRAMERS IONS

The cyclicity definition of Sec. II B can be reformulated in terms of the reduced spin Hamiltonians of the ground- and excited-state hyperfine levels. For non-Kramers ions, the magnetic hyperfine interaction for a singlet electronic state can be described by the Hamiltonian [22]

$$\widehat{H}_{\rm mh} = [\boldsymbol{B}\cdot\boldsymbol{Z}\cdot\boldsymbol{B}]\widehat{\boldsymbol{E}} + \boldsymbol{B}\cdot\boldsymbol{M}\cdot\widehat{\boldsymbol{I}} + \widehat{\boldsymbol{I}}\cdot\boldsymbol{Q}\cdot\widehat{\boldsymbol{I}}, \tag{8}$$

where $\widehat{\boldsymbol{E}}$ is the identity operator, $\widehat{\boldsymbol{I}}$ is the nuclear spin angular momentum operator, $\boldsymbol{B}$ is the applied magnetic field vector, and $\boldsymbol{Z}$, $\boldsymbol{M}$, and $\boldsymbol{Q}$ are the quadratic Zeeman, linear Zeeman, and quadrupole tensors, respectively.

The quadratic Zeeman interaction produces a common frequency shift for all hyperfine states within a particular crystal field level and does not alter the admixtures of the states. Hence, it is ignored.

Another way of posing the question of cyclicity is to ask whether the two matrices representing the ground- and excited-state Hamiltonians $\widehat{H_g}$ and $\widehat{H_e}$, respectively, can be simultaneously diagonalized. If both matrices can be diagonalized in the same basis, then the overlap between the eigenstates $\langle\psi_{e_j}|\psi_{g_k}\rangle$ is unity for $j = k$ and zero otherwise. This is precisely the cyclicity condition defined in Eq. (4).

The ground- and excited-state Hamiltonian terms will be simultaneously diagonalizable, if and only if $\widehat{H_g}$ commutes with $\widehat{H_e}$ [23]. This follows from the fact that $\widehat{H_g}$ and $\widehat{H_e}$ are diagonalizable on the finite-dimensional vector space spanned by I_z.

To provide an illustration of the relationship between the commutation criterion and cyclicity, we first examine sites with axial point group symmetry in zero field.

A. Sites with axial point group symmetry: An example of the commutation criterion in zero field

In zero magnetic field, the spin Hamiltonian for the ground and excited states reduces to the quadrupole term $\widehat{\boldsymbol{I}} \cdot \boldsymbol{Q} \cdot \widehat{\boldsymbol{I}}$. In axial symmetry, the quadrupole tensor $\boldsymbol{Q}$ for any $4f^N$ level is cylindrically symmetric about the rotation axis. In a coordinate system with the z axis along the rotation axis, $\boldsymbol{Q}$ can be written

$$\boldsymbol{Q} = \begin{pmatrix} -\frac{D}{3} & 0 & 0 \\ 0 & -\frac{D}{3} & 0 \\ 0 & 0 & \frac{2D}{3} \end{pmatrix}, \tag{9}$$

where D is the quadrupole parameter of the particular electronic state. This gives a Hamiltonian

$$\widehat{H}_{\mathrm{q}} = D\big({I_z}^2 - \tfrac{1}{3}I(I+1)\big). \tag{10}$$

It can be seen, then, that the ground- and excited-state Hamiltonians are identical except for the scaling parameter D, and therefore must commute. Furthermore, the eigenvectors are the pure I_z states. The cyclicity condition is therefore satisfied for sites with axial symmetry in zero field. Significantly, the spin Hamiltonian given in Eq. (10) holds for all intermediate crystal field levels. Thus, a site with axial symmetry satisfies the condition mentioned at the end of Sec. II C: $|\psi_e\rangle = |\psi_{i_m}\rangle$ for all Γ_i.

An excellent example of a system where the off-diagonal terms of $\widehat{H}_{\mathrm{q}}$ are vanishingly small is Pr^{3+}:$YLiF_4$. In this axial site, hole burning at zero field is not observed, which demonstrates the high cyclicity of the optical transition [24].

We have shown that perfect axial symmetry assures zero-field cyclicity. However, any deviation from axial symmetry will admix the pure I_z states and break the cyclicity condition. Axial sites in some materials demonstrate zero-field hole burning [25], an indication that the cyclicity condition does not completely hold and that the axial symmetry is partially broken.

The aim of this paper is to derive a method to achieve cyclic transitions irrespective of the site's point group symmetry. As it will be shown, this is possible by changing the hyperfine state admixtures through the linear Zeeman interaction. We note here that the quadrupole interaction admixes states with $\Delta I_z = \pm 2$ and the linear Zeeman interaction admixes states with $\Delta I_z = \pm 1$. Therefore, it is not possible to undo the admixing created by the quadrupole interaction by applying a magnetic field. Rather, cyclic optical transitions can only be achieved in the limit where the linear Zeeman interaction strength is far greater than the quadrupole interaction strength: the high-field limit.

B. Derivation of field directions for ZEC

In this section, we consider the high-field limit where the spin Hamiltonian can be approximated by the linear Zeeman interaction. We derive the magnetic field directions along which the spin-state admixtures created by the linear Zeeman interaction are equivalent in the ground and excited states. Thus, in the high-field limit, where the quadrupole contribution is negligible compared to the linear Zeeman term, the transition will approach perfect cyclicity. The following process allows the direction of the ZEC field to be calculated even for the lowest symmetry site.

To calculate the overlap between the eigenvectors of the ground- and excited-state hyperfine Hamiltonians, both Hamiltonians must be expressed in a common coordinate frame. The form of the linear Zeeman tensors in a common coordinate frame can be written as

$$\widetilde{\boldsymbol{M_j}} = R_{Mj} \cdot \boldsymbol{M_j} \cdot {R_{Mj}}^T, \tag{11}$$

where the $\boldsymbol{M_j}$ are the ground- and excited-state linear Zeeman tensors expressed in their respective diagonal bases. The rotation matrices are defined by Euler angles (α,β,γ) [26], which in the general case can be written as $R(\alpha_{Mj},\beta_{Mj},\gamma_{Mj})$. Upon the application of the ZEC field, both the ground- and excited-state Zeeman Hamiltonians could be transformed into a common basis (x_B,y_B,z_B) that diagonalizes both terms.

Let $\boldsymbol{M_g}$ and $\boldsymbol{M_e}$ be the ground- and excited-state linear Zeeman Hamiltonian terms represented in their respective diagonal bases. We choose the basis that diagonalizes $\boldsymbol{M_g}$ as the common basis for our derivation: (x,y,z). In this common basis, the two matrices $\boldsymbol{M_g}$ and $\widetilde{\boldsymbol{M_e}}$ are parametrized according to

$$M_g = \begin{bmatrix} g_x & 0 & 0 \\ 0 & g_y & 0 \\ 0 & 0 & g_z \end{bmatrix}, \tilde{M}_e = \begin{bmatrix} G_1 & G_2 & G_3 \\ G_2 & G_4 & G_5 \\ G_3 & G_5 & G_6 \end{bmatrix}. \tag{12}$$

The relationship between the six components of the $\widetilde{\boldsymbol{M_e}}$ tensor in Eq. (12) depends heavily on the point group symmetry of the rare-earth ion site. As will be detailed in Sec. IV, for sites with higher point group symmetries the number of independent components reduces to a minimum of two for axial symmetry. This significantly reduces the complexity of the commutation criterion compared to the general case required for sites with C_s and C_1 point group symmetry.

In the high-field limit, the commutation criterion for ZEC is written as

$$[(\boldsymbol{B} \cdot \boldsymbol{M_g} \cdot \widehat{\boldsymbol{I}})(\boldsymbol{B} \cdot \widetilde{\boldsymbol{M_e}} \cdot \widehat{\boldsymbol{I}}) - (\boldsymbol{B} \cdot \widetilde{\boldsymbol{M_e}} \cdot \widehat{\boldsymbol{I}})(\boldsymbol{B} \cdot \boldsymbol{M_g} \cdot \widehat{\boldsymbol{I}})] = 0. \tag{13}$$

Upon expanding out the expression in Eq. (13), the ${\widehat{I_x}}^2$, ${\widehat{I_y}}^2$, and ${\widehat{I_z}}^2$ terms cancel, leaving only cross terms. Thus, the equality can be written

$$\begin{aligned}\{&[\widehat{I_x},\widehat{I_y}](B_y g_y u - B_x g_x v) + [\widehat{I_x},\widehat{I_z}](B_z g_z u - B_x g_x w) \\ &+ [\widehat{I_y},\widehat{I_z}](B_z g_z v - B_y g_y w)\} = 0,\end{aligned} \tag{14}$$

where $[\widehat{I}_j,\widehat{I}_k]$ is the normal commutator operation and u, v, and w are given by

$$\begin{aligned} u &= B_x G_1 + B_y G_2 + B_z G_3, \\ v &= B_x G_2 + B_y G_4 + B_z G_5, \\ w &= B_x G_3 + B_y G_5 + B_z G_6. \end{aligned} \tag{15}$$

None of the three terms in square brackets on the left-hand side of Eq. (14) commute. Thus, the condition for achieving ZEC can be reduced to three equations

$$B_y g_y u - B_x g_x v = 0, \tag{16a}$$

$$B_z g_z u - B_x g_x w = 0, \tag{16b}$$

$$B_z g_z v - B_y g_y w = 0 \tag{16c}$$

or explicitly

$$\begin{aligned} &[B_y g_y (B_x G_1 + B_y G_2 + B_z G_3) \\ &\quad - B_x g_x (B_x G_2 + B_y G_4 + B_z G_5)] = 0, \end{aligned} \tag{17a}$$

$$\begin{aligned} &[B_z g_z (B_x G_1 + B_y G_2 + B_z G_3) \\ &\quad - B_x g_x (B_x G_3 + B_y G_5 + B_z G_6)] = 0, \end{aligned} \tag{17b}$$

$$\begin{aligned} &[B_z g_z (B_x G_2 + B_y G_4 + B_z G_5) \\ &\quad - B_y g_y (B_x G_3 + B_y G_5 + B_z G_6)] = 0. \end{aligned} \tag{17c}$$

The field directions that simultaneously diagonalize the ground- and excited-state linear Zeeman Hamiltonians can be calculated by solving the expression in Eq. (17). Because this condition is equivalent to achieving cyclic transitions, the solutions represent the ZEC fields.

IV. ZEC FIELD DIRECTIONS FOR NONCENTROSYMMETRIC SITES WITH A PROPER ROTATION AXIS

A greater understanding of the ZEC technique can be gained by examining the field directions for cyclic transitions for sites possessing particular point group symmetries. The discussion begins by calculating the ZEC field directions for sites with axial point group symmetry. Then, the ZEC field solutions are calculated for the three symmetries that are nonaxial but still possess a proper rotation symmetry axis: D_2, C_{2v}, and C_2. The progression from high to low symmetry is mirrored in the ZEC field directions, which develop in complexity towards the general case: the remaining two noncentrosymmetric point group symmetries C_s and C_1 (see Sec. V).

A. ZEC field directions for sites with axial point group symmetry

In a site with axial point group symmetry, the principal axes of the ground- and excited-state Zeeman tensors coincide and the x and y axes are equivalent and labeled $\perp$. Therefore, $g_x = g_y = g_\perp$, $G_1 = G_4 = G_\perp$, $G_2 = G_3 = G_5 = 0$, and any field in the xy plane is labeled as $B_\perp$. In this case, the expressions in Eq. (17) reduce to one equation

$$B_\perp B_z (g_z G_\perp - g_\perp G_6) = 0. \tag{18}$$

Therefore, the ZEC field solutions are simply fields of the form $(B_\perp,0)$ and $(0,B_z)$. That is, a closed optical transition can be formed by applying a large magnetic field parallel or perpendicular to the z axis of an axial site. Two examples of crystals in which rare-earth ion dopants reside in an axial site are $YLiF_4$ and YPO_4.

B. ZEC field directions for sites with D_2 and C_{2v} point group symmetry

We now examine sites with D_2 or C_{2v} (orthorhombic) point group symmetry. As an example, orthorhombic site symmetry occurs for rare-earth ion dopants in $Y_3Al_5O_{12}$ (YAG) crystals. Like in the axial case, the directions of the three principal axes are common for the ground- and excited-state tensors. However, the x and y principal axes are now distinct. Therefore, $G_2 = G_3 = G_5 = 0$, and the expressions in Eq. (17) become

$$B_x B_y (g_y G_1 - g_x G_4) = 0, \tag{19a}$$

$$B_x B_z (g_z G_1 - g_x G_6) = 0, \tag{19b}$$

$$B_y B_z (g_z G_4 - g_y G_6) = 0. \tag{19c}$$

From the form of the expressions in Eq. (19) the ZEC field solutions can be simply identified as $(B_x,0,0)$, $(0,B_y,0)$, and $(0,0,B_z)$. That is, a closed optical transition can be formed by applying a large magnetic field along any of the three principal axes of the linear Zeeman tensor. This effect has already been discussed in the paper examining Λ transitions in the specific case of Tm^{3+}:YAG [15].

C. ZEC field directions for sites with C_2 point group symmetry

When the site point group symmetry is reduced from orthorhombic to C_2 symmetry, the only common principal axis for both ground- and excited-state linear Zeeman tensors is the z axis. The relationship between the two tensors is then a rotation around the common z axis. In contrast to the orthorhombic symmetry case, $G_2 \neq 0$. The resulting forms of the expressions in Eq. (17) are

$$-{B_x}^2 g_x G_2 + {B_y}^2 g_y G_2 + B_x B_y (g_y G_1 - g_x G_4) = 0, \tag{20a}$$

$$B_z [B_x (g_z G_1 - g_x G_6) + B_y g_z G_2] = 0, \tag{20b}$$

$$B_z [B_y (g_z G_4 - g_y G_6) + B_x g_z G_2] = 0. \tag{20c}$$

For $B_z = 0$, the three equations are satisfied by the solution of Eq. (20a), the form of which is governed by the discriminant

$$\Delta = (g_y G_1 - g_x G_4)^2 + 4 g_x g_y {G_2}^2. \tag{21}$$

If $\Delta < 0$, there are no real solutions apart from the trivial solution $(0,0,0)$. In the specific case where $\Delta = 0$, then there exists one ZEC field direction $(B_x,\mathfrak{m}B_x,0)$ where

$$\mathfrak{m} = \frac{g_x G_4 - g_y G_1}{2 g_x G_2}. \tag{22}$$

Finally, if $\Delta > 0$ then there are two ZEC field directions of the form $(B_x,\widetilde{\mathfrak{m}}B_x,0)$ where

$$\widetilde{\mathfrak{m}} = \frac{g_x G_4 - g_y G_1 \pm \sqrt{\Delta}}{2 g_x G_2}. \tag{23}$$

The case where $B_z \neq 0$ also needs to be considered. The solutions for Eq. (20a) are identical to the $B_z = 0$ case. Equations (20b) and (20c) are satisfied when

$$B_y = \frac{g_x G_6 - g_z G_1}{g_z G_2} B_x \tag{24}$$

and

$$B_y = \frac{g_z G_2}{g_y G_6 - g_z G_4} B_x, \tag{25}$$

respectively. The only solution that satisfies all the expressions in Eq. (20) for $B_z \neq 0$ is $(0,0,B_z)$.

Therefore, in a site with C_2 point group symmetry there will always be at least one magnetic field direction to provide ZEC: a field applied parallel to the site z axis $(0,0,B_z)$. Depending on the site, there may be two, one, or no further ZEC field directions. If these further solutions exist, the required direction will lie in the plane perpendicular to the z axis. Examples of crystals in which rare-earth ions reside in a C_2-symmetric site include Y_2O_3, LaF_3, and $EuCl_3 \cdot 6H_2O$.

V. ZEC IN Pr^{3+}:Y_2SiO_5: A C_1 SITE

In this section, we demonstrate that there are field directions that satisfy the ZEC criterion for site point group symmetries without a proper rotation symmetry (C_s and C_1). Crystals in which such site symmetries occur include $YAlO_3$ and Y_2SiO_5. We achieve this by calculating the ZEC field directions for the lowest site point group symmetry C_1 and, hence, illustrate the general applicability of ZEC for forming closed optical transitions. For sites with C_s or C_1 point group symmetry, there are no restrictions on the form of $\widetilde{\boldsymbol{M}_e}$. This means that it is not possible to generalize the ZEC field solutions for these low-symmetry sites.

Instead, we use the example of the ${}^3H_4 \leftrightarrow {}^1D_2$ transition of site 1 Pr^{3+}-ion dopants in Y_2SiO_5, a material of significant interest for both quantum information applications [7,27,28] and single-ion detection [29]. To begin with, the ZEC field directions for this low-symmetry site are calculated. We then calculate the transition probabilities for a field applied along the ZEC field directions taking both the quadrupole and linear Zeeman interactions into consideration.

There is strong evidence that site 1 ions in Pr^{3+}:Y_2SiO_5 satisfy the diabatic criterion presented in Sec. II C. In particular, studies have demonstrated that there is strong agreement between high-frequency resolution hole burning spectra and models based on the transition probabilities of the direct ${}^3H_4 \leftrightarrow {}^1D_2$ transition [32]. The agreement between the experiment and model demonstrates that indirect relaxation pathways do not significantly perturb the hyperfine state of the ions. If Pr^{3+}:Y_2SiO_5 does not fulfill the diabatic criterion, the analysis included in this section still demonstrates the existence of ZEC field directions in sites with C_1 symmetry. Furthermore, the calculations in Sec. V A indicate the degree to which the optical transition probabilities in rare-earth ion materials can be engineered to approach unity in the high-field limit. The calculated transition probabilities represent the possible level of cyclicity in materials suitable for ZEC (see Sec. VII A).

TABLE I. Spin Hamiltonian parameters for Pr^{3+}:Y_2SiO_5 (site 1) as measured by Lovrić *et al.* [30].

	Ground state ${}^3H_4$ Value	Excited state ${}^1D_2$ Value
D	−4.4435 MHz	1.35679 MHz
E	−0.56253 MHz	0.42192 MHz
α_Q	62.1°	123.51°
β_Q	31.81°	94.69°
γ_Q	93.94°	170.56°
g_x	26.57 MHz/T	14.54 MHz/T
g_y	31.01 MHz/T	14.30 MHz/T
g_z	113.08 MHz/T	33.76 MHz/T
α_M	112.0°	44°
β_M	35.68°	63.91°
γ_M	101.54°	3°
α_{C_2}	110.0°	120°
β_{C_2}	1.574°	1.65°

Table I details the parameters for the ground- and excited-state quadrupole and linear Zeeman Hamiltonian parameters as determined by Lovrić *et al.* [30]. The ground- and excited-state linear Zeeman tensors $\boldsymbol{M_g}$ and $\widetilde{\boldsymbol{M_e}}$, respectively, can be written in the basis that diagonalizes $\boldsymbol{M_g}$:

$$M_g = \begin{bmatrix} 26.57 & 0 & 0 \\ 0 & 31.01 & 0 \\ 0 & 0 & 113.08 \end{bmatrix},$$
$$\tilde{M}_e = \begin{bmatrix} 23.60 & 8.85 & 3.71 \\ 8.85 & 23.17 & 3.67 \\ 3.71 & 3.67 & 15.83 \end{bmatrix}. \tag{26}$$

When these two Zeeman tensors are fed into the expressions in Eq. (17), three solutions are found for the case where $B_z \neq 0$, while no solutions exist for $B_z = 0$. The ZEC field directions for Pr^{3+}:Y_2SiO_5 are plotted in the commonly used (D_1, D_2, C_2) coordinate frame [18] in Fig. 2. The three solutions are

$$[B_{D_1}, B_{D_2}, B_{C_2}] = \begin{cases} [-0.81, 0.16, 0.56] & \text{(i)}, \\ [0.59, 0.29, 0.75] & \text{(ii)}, \\ [0.02, -0.98, 0.18] & \text{(iii)}. \end{cases} \quad \text{and} \tag{27}$$

It is interesting to note that the three ZEC field directions are almost mutually orthogonal, which suggests a deeper underlying symmetry to this ZEC analysis. This would be an interesting subject of further study beyond this work.

A. Predicted performance of the ZEC technique

The ZEC technique predicts perfect cyclicity in the limit of an infinitely large magnetic field. Having established the existence and values of ZEC field directions for Pr^{3+}:Y_2SiO_5 in the previous section, the performance of the technique as we approach the infinite field limit is now calculated. To investigate the upper bound on the level of cyclicity induced by a large applied field in the directions calculated by the analysis above, the transition probabilities $|\langle\psi_e|\psi_g\rangle|^2$ are calculated as a function of magnetic field strength. The

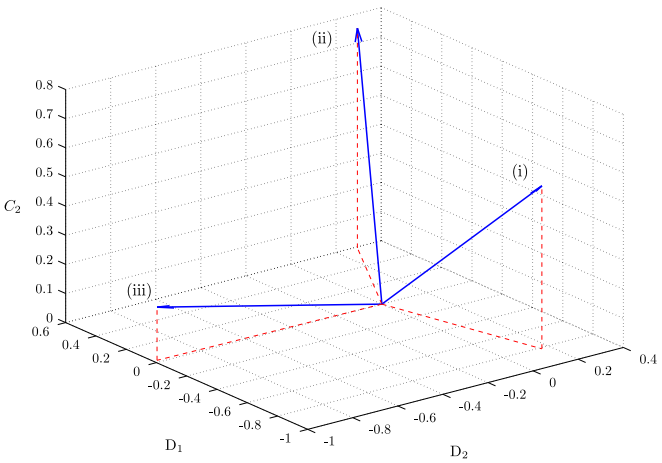

FIG. 2. ZEC field directions for Pr^{3+}:Y_2SiO_5 (site 1), labeled (i), (ii), and (iii), in the (D_1, D_2, C_2) coordinate frame.

hyperfine Hamiltonians, including both quadrupole and linear Zeeman terms, are calculated for each magnetic field value. The eigenvalues and corresponding eigenvectors $|\psi_g\rangle$ and $|\psi_e\rangle$ of the Hamiltonian matrices are then used to calculate the transition probability for each of the 36 ground- and excited-state combinations.

To provide a reference for the ZEC field calculations, the transition probability matrix for Pr^{3+}:Y_2SiO_5 in zero field is shown in Fig. 3. Because the quadrupole interaction significantly mixes the pure $\boldsymbol{I}_z$ states, the hyperfine structure is identified by the labels 1 through to 6: 1 being the lowest-energy level and 6 being the highest. In zero field, levels (1 and 2), (3 and 4), and (5 and 6) are degenerate for both the ground and excited states.

Figure 3 illustrates the mixing due to the quadrupole term in this material. For example, the transition probabilities among states 3–6 are, to a large extent, independent of the levels involved. In contrast, there is one transition that exists in zero field that exceeds 90% likelihood: the (1,2)g $\leftrightarrow$ (1,2)e. Although large compared to the other zero-field transitions, this level of cyclicity is insufficient for high-fidelity readout schemes, which require closer to 99.99% transition probabilities [31].

We note that although the spin Hamiltonian parameters calculated by Lovrić *et al.* [30] achieve excellent agreement with the experimentally observed oscillator strengths [32], the relative frequencies of these transitions are incorrect. From the zero-field experimental results of Nilsson *et al.* [32], the strongly selective transitions would be labeled by energy as (1,2)g $\leftrightarrow$ (5,6)e rather than as they appear in Fig. 3: (1,2)g $\leftrightarrow$ (1,2)e.

The most likely explanation for this discrepancy is the configuration of the $\boldsymbol{Q}$-tensor principal axes chosen in Lovrić's paper. Clarification of the parameters for Pr^{3+}:Y_2SiO_5 is in progress to determine the correct configuration. However, to maintain consistency with the published literature in the absence of any revision at the time of writing, the parameters from Ref. [30] are used. In the high-field regime in which the ZEC protocol operates, the impact of the correct quadrupole parameters on the transition cyclicity will be very small. Therefore, the results presented in this paper are largely independent of any future disambiguation of the quadrupole parameters.

Figures 4–6 illustrate the calculated enhancement of the transition probabilities when a large magnetic field is applied along ZEC field direction (i) [see Eq. (27) and Fig. 2]. The calculated transition probabilities with ZEC fields applied along directions (ii) and (iii) are similar to the presented results. Figure 4 plots the evolution of the ground- and excited-state hyperfine level frequencies as the magnetic field is increased to 1 T along direction (i). The nonlinear behavior at low field is due to the interaction between the quadrupole and the linear Zeeman terms and is indicative of the changing admixtures of

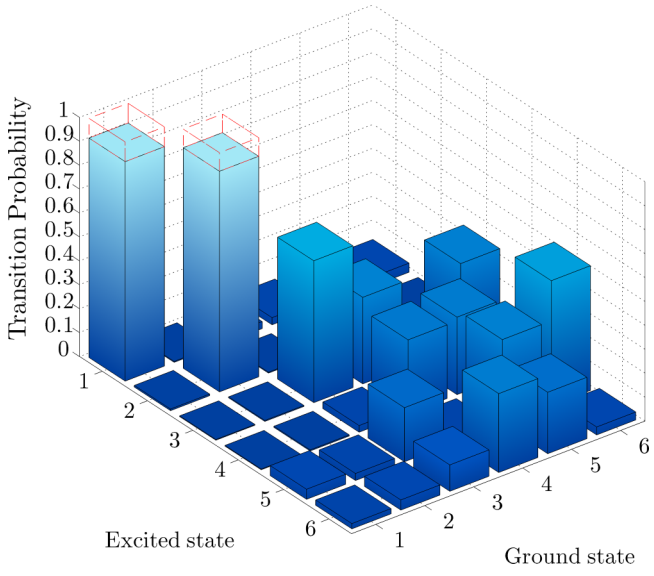

FIG. 3. Transition probabilities for relaxation from the $^1D_2$ excited state to the $^3H_4$ ground state of Pr^{3+}:Y_2SiO_5 (site 1) in zero magnetic field. The hyperfine levels are labeled according to their energy: 1 for the lowest-energy level and 6 for the highest.

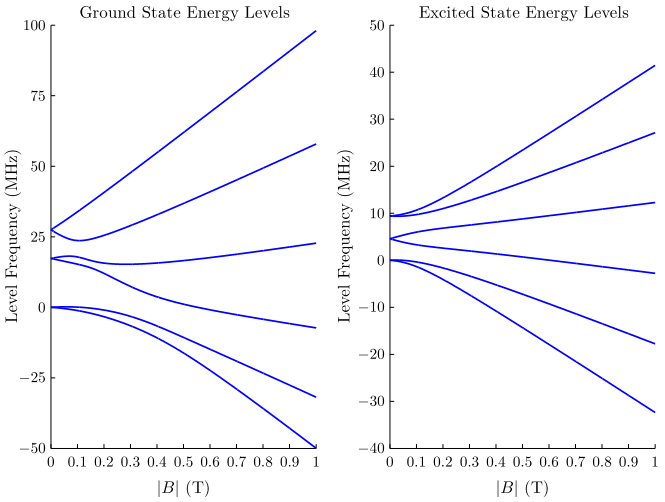

FIG. 4. Hyperfine level frequencies as the field magnitude is increased along ZEC field (i). The frequency is plotted as an offset from the lowest hyperfine level in zero field for the ground ($^3H_4$) and excited ($^1D_2$) states, respectively. The ordering of the hyperfine levels agree with the experimental results of Ref. [32].

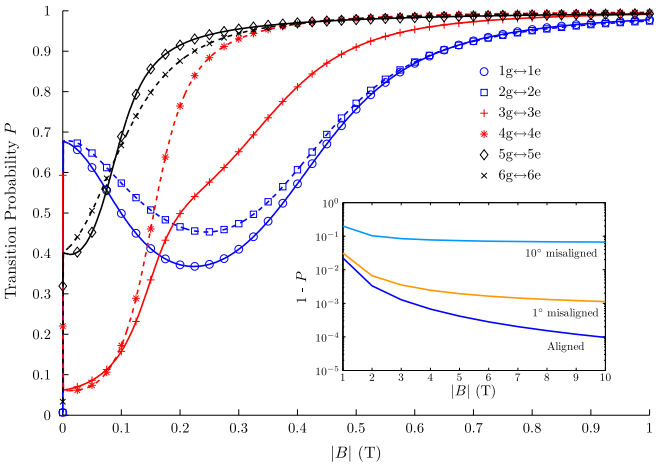

FIG. 5. Evolution of the transition probabilities P for the like-to-like transitions as the magnetic field magnitude is increased along ZEC field (i). The main figure shows that the P for all six transitions approaches unity at 1 T. The inset shows the value of $1 - P$ for the most cyclic like-to-like transition as a function of field strength and alignment.

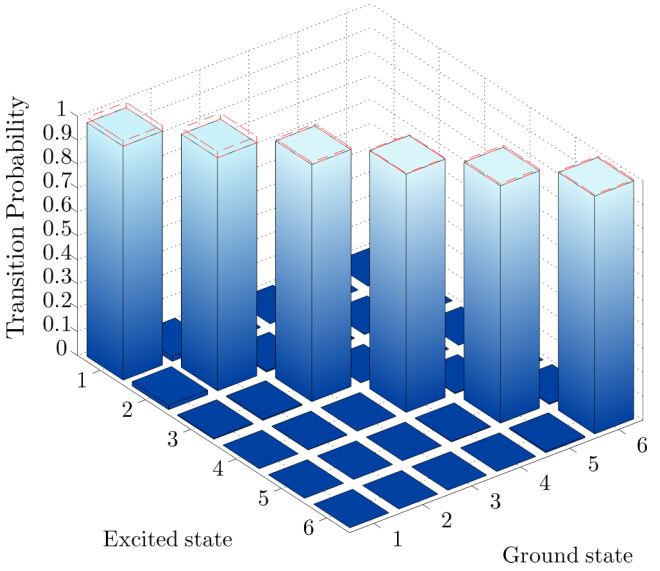

FIG. 6. Transition probabilities for relaxation from the $^1D_2$ excited state to the $^3H_4$ ground state of Pr^{3+}:Y_2SiO_5 (site 1) for a 1-T field applied along ZEC field (i).

the states. As the field increases above 0.5 T, the behavior of all the hyperfine levels trends towards the linearity dictated by the dominant Zeeman term.

Figure 5 shows the transition probabilities P for the like-to-like transitions as the field strength is increased. The like-to-like transitions are defined via the level energies, giving the $1g \leftrightarrow 1e$ transition as the lowest-to-lowest transition. For very small fields, the transition probabilities change rapidly due to the introduction of the linear Zeeman term. Above approximately 0.5 T, the probabilities of all the transitions asymptotically approach unity. This demonstrates the desired ZEC effect for Pr^{3+}:Y_2SiO_5.

The inset in Fig. 5 plots $(1 - P)$ as the field strength is increased to 10 T for three levels of field alignment. As shown, for a perfectly aligned ZEC field at 10 T the probability of optically inducing a hyperfine state transition is 10^{-4}. Even with a misalignment of 1° at 10 T, an order of magnitude decrease compared to the zero-field value of $(1 - P)$ can be achieved. If the field is misaligned at the 10° level, the transition probabilities for the six like-to-like transitions are approximately equal to the best performing zero-field transition: $(1 - P) \approx 0.05$.

To highlight the improvements offered by the ZEC technique, Fig. 6 shows the complete transition probability matrix for a 1-T field applied along direction (i). This is a stark contrast to the zero-field probabilities illustrated in Fig. 3. The strong selectivity of the like-to-like transitions is emphasized, as the diagonal elements are all close to unity. Correspondingly, the off-diagonal elements are vanishingly small.

VI. APPLICATIONS OF ZEC IN RARE-EARTH MATERIALS

The primary motivation for proposing ZEC for rare-earth ion systems is to achieve single-ion, state-selective readout, which we describe in this section. In addition, the ability to tune the transition probabilities via magnetic fields has applications for many protocols that involve Λ systems in rare-earth ion materials. These include both the gradient echo memory (GEM) [7] and atomic frequency comb (AFC) [8] quantum memory protocols as well as classical data storage. The example provided in this section is the application of the ZEC technique to create write-once, read-many (WORM) spectral features that can be applied for classical and quantum data storage and processing.

A. Single-ion state-selective readout

Definitive optical detection of a single rare-earth ion has only recently been achieved [29,33,34]. The ZEC technique extends the work contained in Refs. [29,33,34] by establishing a feasible method for achieving hyperfine-state-selective readout at the single-ion level. By engineering cyclic transitions, the ion can be repeatedly optically excited from a single hyperfine ground state. As a result, the presence or absence of a fluorescent signal can be used to determine the nuclear spin of the single ion. Such a readout scheme is a critical element for frequency-based, single-ion qubit quantum computing proposals in rare-earth ion systems.

An important question is whether a hyperfine state readout technique using ZEC can achieve a high level of fidelity. In Sec. V A, the ZEC protocol was simulated to create transition probabilities of the order of 99.99%. For common rare-earth ion excited state lifetimes (100 μs − 1 ms), this would result in the emission of 10^4 photons during a period ranging between 1–10 s. These photons must be collected and detected, which incurs losses. The collection efficiency exceeding 50% achieved in Ref. [29] indicates that 10% total efficiency in fluorescence detection is possible for isolated ions in a bulk crystal. Therefore, a feasible number of detection events when the ion is in the targeted ground-state hyperfine level is 10^3.

To determine the state of the single ion, the fluorescent signal must be able to be differentiated from the absence of fluorescence that indicates that the ion is in another hyperfine ground state. To approximate the achievable signal-to-noise ratio of this measurement, we assume that the only additional noise source is the dark counts from the detector. Avalanche photodiodes with dark count rates of the order of 1 count per second are commercially available for the emission wavelengths of praseodymium and europium. Therefore, for integration over the period where the ion remains cyclic, the number of dark counts would be described by a Poissonian distribution with mean total counts $\langle n \rangle \approx 10$. In contrast, the signal from a resonant single ion would be described by a Poissonian distribution with mean total counts $\langle n \rangle \approx 10^3$. Distinguishing between these two distributions, which corresponds to a fluorescence-based measurement of the ion's hyperfine ground state, can be achieved with an error less than 10^{-5} [[31] pp. 49–51].

Therefore, by combining high optical detection efficiency with the ZEC technique, it is feasible to achieve high-fidelity single-ion state readout. As a consequence, the ZEC technique represents a significant opportunity for increasing the scale of rare-earth ion quantum computing [35,36].

B. WORM spectral features

Many applications for trivalent rare-earth ions in crystals are centered on the ability to harness Λ systems to create specific spectral features. For example, there is continuing interest in using rare-earth ion crystals as frequency references by creating single, isolated depleted regions in the absorption profile (holes) [13]. An example of a more complex spectral structure is the combs created for AFC quantum memory protocols [37]. These and other similar spectral features are often created by manipulating the population of ions among the ground-state hyperfine levels.

Once spectral features are written into the inhomogeneously broadened transition of an ensemble through optical pumping, the long lifetimes of the hyperfine ground states ensure that the structures can remain for hours to days [2]. However, if the spectral feature undergoes further optical excitation, the structure is quickly degraded because of optically induced changes in the spin state. The result is that spectral features must be repetitively created between processing steps to ensure that the system is initialized correctly at each point in the protocol.

The ZEC protocol proposed in this paper could be applied to prepare a WORM spectral feature. That is, a feature optically prepared in the inhomogeneous line could be engineered to be robust against optical excitation. According to the theoretical calculations outlined in this paper, through the application of a ZEC field a spectral feature could be probed 10^4 times with high-excitation probability before degrading significantly. Furthermore, in the regime of low-excitation probability, the feature could remain on time scales where the hyperfine state lifetime rather than optical excitation effects limit the feature stability. Such features would have applications in many areas including frequency references [6], classical [4] and quantum [7,8] memories, nonclassical light sources [9], and other protocols utilizing Λ systems in rare-earth materials.

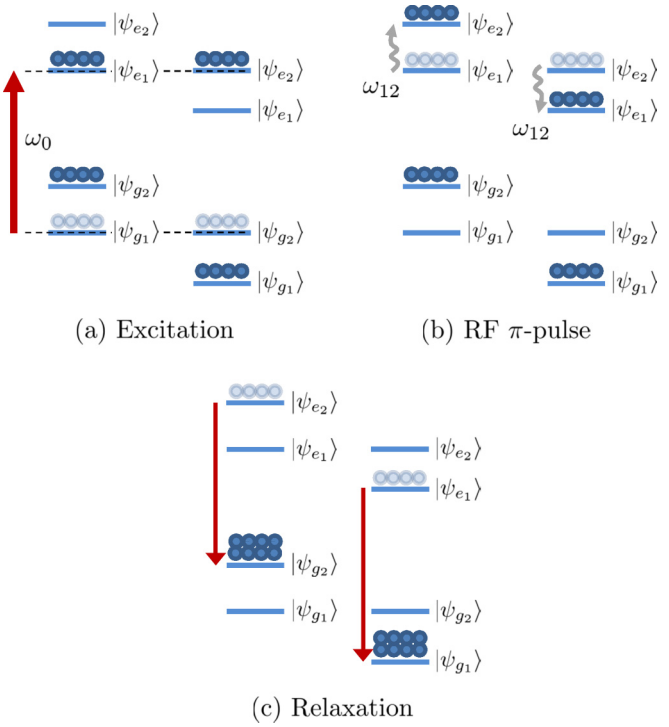

FIG. 7. A technique to create WORM spectral features in the presence of strongly favored like-to-like transitions created by ZEC. Ions are optically excited at frequency ω_0, which excites all like-to-like transitions for a subset of ions within an inhomogeneously broadened absorption profile. The application of a π pulse at ω_{12} changes the hyperfine state of all the excited ions. When the ions relax, the initial ground-state hyperfine population distribution is significantly altered.

One technique for writing a WORM feature is illustrated in Fig. 7. The proposed technique uses a combination of optical excitation and radio-frequency (rf) pulses to write the feature in the presence of strongly favored like-to-like transitions. The basis of this technique has been applied in optically detected nuclear spin resonance experiments in axially symmetric sites [24] and also to enhance optical pumping in poor Λ systems [38]. To create a hole, the ions resonant at an excitation frequency ω_0 are optically pumped to the excited state. In a time short compared to the excited-state lifetime, a rf π pulse is applied, which is resonant with the excited-state hyperfine splittings ω_{12}. Following the rf pulse, none of the optically excited ions reside in the hyperfine levels to which they were excited. After a time long compared to the lifetime of the optical excited state, the ions will have relaxed back to the ground state. The result is a depleted absorption feature at ω_0 because of the high probability of the like-to-like transitions. The strongly cyclic transitions also allow the spectral region around the hole to be optically probed repeatedly without inducing changes in the ground-state hyperfine populations. Therefore, the feature can be preserved despite optical interactions. Although Fig. 7 illustrates the technique for spin-$\frac{1}{2}$ ions, the procedure is easily extended to higher-spin systems

through further rf π pulses at excited-state hyperfine transition frequencies.

VII. CONSIDERATIONS FOR THE EXPERIMENTAL REALIZATION OF ZEC

To supplement the theoretical aspects of this paper, in this section we briefly discuss three experimental considerations when using ZEC to close optical transitions. We first describe in more detail which materials are suitable for the proposed technique. We then discuss the requirements and optimization of the applied magnetic field. Finally, we consider the consequences of hyperfine parameter inhomogeneity in the applications of the ZEC technique.

A. Rare-earth ion materials suitable for ZEC

In Sec. II C, we showed that the crystals in which relaxation from the optical excited state can be treated as a diabatic passage are suitable candidates for ZEC. For these materials, the only relaxation pathways from $|\Gamma_e\rangle|\psi_e\rangle$ to $|\Gamma_g\rangle|\psi_{g_n}\rangle$ that exist fulfill the diabatic criterion $\tau \ll \omega_m^{-1}$. Although there are many promising materials that satisfy this criterion, the range of materials suitable for ZEC can be expanded considerably by considering the ion's electronic structure and its site point group symmetry.

The electronic component of Eq. (3) governs the transition probabilities between the electronic states Γ. This branching ratio weights the contribution of each indirect relaxation path towards the total probability of terminating in a particular hyperfine spin state. Therefore, even if metastable states exist that would violate the diabatic criterion, it is possible that the branching ratio for indirect relaxation paths containing these states is negligible. This increases the number of materials in which cyclicity can be controlled by manipulating $\langle\psi_e|\psi_g\rangle$.

If relaxation pathways exist that contain metastable levels and possess non-negligible branching ratios, the ZEC method can still be successful. If all the relevant intermediate crystal field level spin Hamiltonians can be simultaneously diagonalized (equivalent to requiring $|\psi_e\rangle = |\psi_{i_m}\rangle$ for all Γ_i), then the initial hyperfine spin state will be preserved irrelevant of the relaxation path. This criterion is easily fulfilled in sites with a proper rotation axis of symmetry. For sites with point group symmetries higher than C_s, the relaxation path-independent ZEC can be realized if the ZEC field is applied along any common principal axis.

We conclude this discussion by summarizing the non-Kramers crystals suitable for closing optical transitions using the ZEC technique. First, if the site possesses a proper rotation axis, then at least one ZEC field direction will provide enhanced cyclicity. For sites with C_s or C_1 point group symmetry, the ZEC technique should succeed if all indirect relaxation pathways fulfill the diabatic criterion, or indirect pathways containing a metastable state possess negligible branching ratios. The large number of crystals for which the technique is applicable makes it an appealing protocol for fundamental and applied rare-earth ion spectroscopy.

1. A comment on ZEC in crystals containing Kramers ions

In this paper, we have restricted our focus to non-Kramers ions, but the natural next step is to consider the application of ZEC to crystals containing Kramers ions. Here, we provide a few brief comments on achieving closed optical transitions in Kramers-ion systems as a starting point for a more complete analysis in the future.

For a Kramers ion with zero nuclear spin, the spin Hamiltonian $\widehat{H}_{\rm mh}$ of a Kramers doublet only contains the linear (electronic) Zeeman interaction [13]

$$\widehat{H}_{\rm mh} = \beta \boldsymbol{B} \cdot \boldsymbol{g} \cdot \widehat{\boldsymbol{S}}, \tag{28}$$

where β is the electronic Bohr magneton, $\boldsymbol{B}$ is the applied magnetic field vector, $\boldsymbol{g}$ is the g factor of the Kramers doublet, and $\widehat{\boldsymbol{S}}$ is the spin-$\frac{1}{2}$ operator. The form of $\widehat{H}_{\rm mh}$ in Eq. (28) is mathematically equivalent to the spin Hamiltonian of the non-Kramers ion Tm^{3+}, which has $I = \frac{1}{2}$. If the cyclicity condition in Eq. (4) is expressed using electron-spin states rather than nuclear-spin states, the commutation criterion presented in Sec. III B can be applied by substituting the appropriate $\boldsymbol{g}$ tensors for $\boldsymbol{M_g}$ and $\boldsymbol{M_e}$. Therefore, the general results of Secs. IV and V hold for Kramers ions with $I = 0$. This is supported by the conclusions of Ref. [39] where the branching ratio of Λ transitions in Nd^{3+}:YVO_4 are found to be zero when a field is applied parallel or perpendicular to the crystal symmetry axis.

For Kramers-ion isotopes with $I \neq 0$, both the electron- and nuclear-spin interactions must be taken into consideration. This case can be simplified by noting that the tensors that describe these different spin interactions will all possess a principal axis along the symmetry axis of the rare-earth ion site (if one exists). Therefore, following the logic of Sec. IV, for noncentrosymmetric sites possessing a proper rotation axis, ZEC fields will exist parallel to the symmetry axis of the site. As for sites with no proper rotation axis (C_s or C_1), it is unclear whether ZEC fields will exist.

Although ZEC field directions will exist for some Kramers-ion systems, the achievable cyclicity enhancement needs to be examined in detail, which is beyond the scope of this work. For example, the level of cyclicity that can be obtained will depend on the lifetime of the electron-spin states, which is typically much shorter than the lifetime of nuclear-spin states [38,39]. Furthermore, the diabatic criterion presented in this work will be significantly harder to fulfill. This is because the energy splittings between the electron-spin states can be several orders of magnitude larger than the splittings between nuclear-spin states.

B. Applied magnetic field

Because the performance of the ZEC technique relies on working in the high-field limit, the properties of the applied field are an important factor in closing optical transitions. The magnitude, orientation, and homogeneity of the field will contribute to the achievable level of cyclicity. Realizing the magnetic field parameters for high-performance ZEC is certainly feasible given the success of the significantly more demanding zero first-order Zeeman (ZEFOZ) technique [3].

To achieve the maximum possible cyclicity, the field magnitude along the ZEC direction should be maximized. In this work, fields up to 10 T were considered but the calculations highlight that rapid gains in cyclicity can be made for field magnitudes up to approximately 3 T. Although cyclicity continues to improve as the field strength is increased, the rate of increase diminishes.

For experiments applying fields less than $\approx$5 T it will be important to factor in the finite contribution of the quadrupole interaction when optimizing the field alignment. The calculations performed in Sec. V A simply show the level of cyclicity for fields applied along the direction derived in the high-field limit. For field strengths below $\approx$5 T, the maximum cyclicity may be achieved on the order of 1° away from the ZEC field direction. The optimum direction can be found by performing a numerical search in the magnetic field space around the theoretical ZEC field.

In general, the enhancement of cyclicity relies on the linear Zeeman interaction dominating the quadrupole interaction. How strong a field is required to attain the high-field limit is then governed by the relationship between the eigenstates of the quadrupole interaction and the eigenstates of the linear Zeeman interaction. We have explored this concept using first-order perturbation theory in Appendix B.

Here, we summarize the results of Appendix B. For a site with perfect axial point group symmetry, the quadrupole eigenstates are identical to the linear Zeeman eigenstates. In this case, any field magnitude along a ZEC field direction will produce transition probabilities equal to unity. For other site symmetries, the eigenstates of the quadrupole and linear Zeeman interactions differ. In these cases, only an infinite field applied along a ZEC field direction can produce transition probabilities equal to unity. For nonaxial sites, it is possible to estimate the transition probabilities possible for an applied field along a ZEC field direction using the following expression (derived in Appendix B):

$$|\langle\psi_e|\psi_g\rangle|^2 \geqslant \left(\frac{\lambda_e\lambda_g + 1}{\left(\lambda_e{}^2 + 1\right)^2\left(\lambda_g{}^2 + 1\right)^2}\right)^2 \tag{29}$$

for

$$\lambda_j = |E_{j_q}/E_{j_z}|, \tag{30}$$

where j represents the excited state (e) or the ground state (g), and $|E_q/E_z|$ is the ratio of the quadrupole interaction energy and the linear Zeeman interaction energy for a particular $|\psi_j\rangle$.

C. Hyperfine parameter variation

A final consideration in the factors important for experimentally achieving ZEC is the homogeneity of the hyperfine parameters. Due to spatially dependent variations in the crystal field, individual ions possess different quadrupole and linear Zeeman properties. Equivalently, in an ensemble of ions there will be inhomogeneities in both the $\boldsymbol{Q}$ and $\boldsymbol{M}$ tensors. The variations in the $\boldsymbol{Q}$ tensor will not alter the direction of the required ZEC field but will modify the resultant transition probabilities. In contrast, the result of variations in the $\boldsymbol{M}$ tensor is that each ion or subensemble will possess a unique ZEC field direction.

In most materials, the variations in the $\boldsymbol{Q}$ and $\boldsymbol{M}$ tensors will be small, a fact that is highlighted by the success of other techniques reliant on the hyperfine Hamiltonian parameters. For example, the ZEFOZ technique is much more sensitive to variations in $\boldsymbol{Q}$ and $\boldsymbol{M}$ than ZEC, yet it has been successfully demonstrated in several rare-earth materials [3,40]. In addition, optimization of the magnetic field required for ZEC is experimentally possible by measuring the relevant transition probabilities as a function of field orientation.

VIII. CONCLUSION

A technique that allows the engineering of closed optical transitions in non-Kramers rare-earth ion crystals was proposed and investigated. The technique is based on the manipulation of the ion's hyperfine state admixtures through the application of specifically oriented, large magnetic fields. When the spin Hamiltonians of the ground and excited states possess the same eigenstates, cyclic transitions are formed that allow an optical transition to be closed.

A complete justification of the ZEC technique was given and a derivation of the ZEC field directions was performed. General solutions were examined for sites with axial, orthorhombic, and C_2 point group symmetry. Sites without a proper rotation axis were also investigated through the example of Pr^{3+}:Y_2SiO_5: a C_1 symmetric site. A quantitative analysis performed for Pr^{3+}:Y_2SiO_5 showed that transition probabilities exceeding 99.99% are theoretically possible at 10 T.

Two applications of the ZEC technique were discussed: single-ion, state-selective readout and the creation of WORM spectral features. Given the simulated level of cyclicity enhancement, high-fidelity single-ion qubit readout is feasible under realistic experimental conditions. This result adds weight to the investigation of single rare-earth ions for quantum information processing. Ensemble-based protocols would also benefit from creating spectral features that are robust against optical excitation, which the ZEC technique makes possible.

The engineering of closed optical transitions through the ZEC protocol is a further technique to add to the quantum control that can be achieved in rare-earth ion systems. Critically, it enables the investigation of processes currently impossible for rare-earth ion crystals both in the single-ion and ensemble regimes.

ACKNOWLEDGMENTS

This work was supported by the Australian Research Council Centre of Excellence for Quantum Computation and Communication Technology (Grant No. CE110001027). M.J.S. was supported by an Australian Research Council Future Fellowship (Grant No. FT110100919).

APPENDIX A: DERIVING THE DIABATIC CONDITION

In Sec. II C, a diabatic condition for the preservation of an ion's spin upon indirect relaxation is stated. The purpose of this appendix is to explicitly derive this condition. First, let the direct relaxation path from $|\Gamma_e\rangle|\psi_e\rangle \rightarrow |\Gamma_g\rangle|\psi_{g_n}\rangle$ be

considered. In the excited state $|\Gamma_e\rangle$ the state $|\psi_e\rangle$ is an eigenstate of the Hamiltonian $\widehat{H}_e$,

$$\widehat{H}_e|\psi_e\rangle = E_e|\psi_e\rangle, \tag{A1}$$

where E_e is the energy of the $|\psi_e\rangle$ hyperfine state.

Similarly, the hyperfine levels $|\psi_{g_n}\rangle$ of the ground state Γ_g are governed by

$$\widehat{H}_g|\psi_{g_n}\rangle = E_{g_n}|\psi_{g_n}\rangle, \tag{A2}$$

where $\widehat{H}_g$ and E_{g_n} are the Hamiltonian and energies for the ground states $|\psi_{g_n}\rangle$.

When the ion relaxes to a different electronic level, the hyperfine Hamiltonian changes from $\widehat{H}_e$ to $\widehat{H}_g$. The state $|\psi_e\rangle$ is initially unchanged, but can be expressed in the basis states of the ground-state Hamiltonian as

$$|\psi_e\rangle = \sum_m c_{g_m}|\psi_{g_m}\rangle, \tag{A3}$$

where the $c_{g_m} = \langle\psi_{g_m}|\psi_e\rangle$.

In the Schrödinger picture, the time evolution of this superposition state can then be described by

$$\begin{aligned} |\Psi(0)\rangle &= |\psi_e\rangle = \sum_m c_{g_m}|\psi_{g_m}\rangle, \\ |\Psi(t)\rangle &= \sum_m c_{g_m} e^{-i\omega_m t}|\psi_{g_m}\rangle, \end{aligned} \tag{A4}$$

where $\omega_m = E_{g_m}/\hbar$. If a measurement is made after time τ to ascertain the hyperfine ground state, the relative probabilities $\Pr_{|\psi_e\rangle\to|\psi_{g_n}\rangle}$ are given by

$$\begin{aligned} \Pr_{|\psi_e\rangle\to|\psi_{g_n}\rangle} &= |\langle\Psi(\tau)|\psi_{g_n}\rangle|^2 = \left|\sum_m c^*_{g_m} e^{i\omega_m\tau}\langle\psi_{g_m}|\psi_{g_n}\rangle\right|^2 \\ &= |c^*_{g_n} e^{i\omega_n\tau}|^2 = |\langle\psi_e|\psi_{g_n}\rangle|^2, \end{aligned} \tag{A5}$$

which is independent of the time τ.

However, as previously noted, the dominant relaxation path to the ground state is a complex route through higher-energy crystal field levels. Therefore, let an indirect relaxation path through the intermediate electronic state $|\Gamma_i\rangle$ be considered. Analogous to Eq. (A3), the initial state $|\psi_e\rangle$ can be expressed as a superposition of the basis states of the intermediate state Hamiltonian $\widehat{H}_i$:

$$|\psi_e\rangle = \sum_m c_{i_m}|\psi_{i_m}\rangle, \tag{A6}$$

where the $c_{i_m} = \langle\psi_{i_m}|\psi_e\rangle$. While the ion remains in state $|\Gamma_i\rangle$, the time evolution of the state is given by

$$|\Psi(t)\rangle = \sum_m c_{i_m} e^{-i\omega_m t}|\psi_{i_m}\rangle, \tag{A7}$$

where ω_m is now given by $E_{i_m}/\hbar$. After time τ_i the ion relaxes from Γ_i to Γ_g and each term in the superposition has accumulated a phase $e^{-i\omega_m\tau_i}$. The probabilities $\Pr_{|\psi_e\rangle\to|\Gamma_i\rangle\to|\psi_{g_n}\rangle}$ are given by

$$\begin{aligned} \Pr_{|\psi_e\rangle\to|\Gamma_i\rangle\to|\psi_{g_n}\rangle} &= |\langle\Psi(\tau_i)|\psi_{g_n}\rangle|^2 \\ &= \left|\sum_m c^*_{i_m} e^{i\omega_m\tau_i}\langle\psi_{i_m}|\psi_{g_n}\rangle\right|^2. \end{aligned} \tag{A8}$$

If $\tau_i \ll \max(\omega_m{}^{-1})$, the phase evolution factors $e^{i\omega_m\tau_i} \approx 1$ giving

$$\begin{aligned} \Pr_{|\psi_e\rangle\to|\Gamma_i\rangle\to|\psi_{g_n}\rangle} &= \left|\sum_m c^*_{i_m}\langle\psi_{i_m}|\psi_{g_n}\rangle\right|^2 \\ &= |\langle\psi_e|\psi_{g_n}\rangle|^2. \end{aligned} \tag{A9}$$

Thus, if relaxation to the ground state through an intermediate crystal field level is sufficiently rapid [$\tau_i \ll \max(\omega_m{}^{-1})$], the hyperfine state does not undergo any evolution. The resulting transition probability of terminating in ground state $|\psi_{g_n}\rangle$ is equal to the direct transition given in Eq. (A5). This can be considered as a diabatic passage [19]. The diabatic criterion can be extended to indirect relaxation pathways containing multiple intermediate states. In this case, the lifetime τ_j of every intermediate state $|\Gamma_j\rangle$ traversed in the relaxation process must obey the condition $\tau_j \ll (\omega_m)^{-1}$ for $m = 1 \ldots 2I + 1$.

APPENDIX B: FIRST-ORDER PERTURBATION THEORY ANALYSIS FOR ZEC

Here, we treat the quadrupole interaction $\widehat{H}_\mathrm{q}$ as a perturbation to the linear Zeeman interaction $\widehat{H}_\mathrm{Z}$ for a large magnetic field applied along one of the ZEC field directions. We work in the eigenstate basis that simultaneously diagonalizes the ground- and excited-state linear Zeeman Hamiltonians

$$\widehat{H}_\mathrm{Z}|\psi_n\rangle = E_n|\psi_n\rangle. \tag{B1}$$

According to first-order, time-independent perturbation theory

$$(\widehat{H}_\mathrm{Z} + \lambda\widehat{H}_\mathrm{q})|\Psi_n\rangle \approx E'_n|\Psi_n\rangle, \tag{B2}$$

where

$$\begin{aligned} |\Psi_n\rangle &= \lambda\sum_{k\neq n}\frac{\langle\psi_k|\widehat{H}_\mathrm{q}|\psi_n\rangle}{E_n - E_k}|\psi_k\rangle + |\psi_n\rangle \\ &= \lambda\sum_{k\neq n}\frac{\alpha_{kn}}{\Delta E_{kn}}|\psi_k\rangle + |\psi_n\rangle \end{aligned} \tag{B3}$$

and

$$\lambda = |E_q/E_n|, \tag{B4}$$

where E_q is of the order of the zero-field quadrupole splittings.

The perturbed eigenstates for both the ground and excited crystal field levels can be written in the form of Eq. (B3). The normalized eigenstates $|\Psi_{e_n}\rangle$ and $|\Psi_{g_n}\rangle$ are

$$|\Psi_{e_n}\rangle = \frac{\lambda_e\sum_{k\neq n}\frac{\alpha_{e_{kn}}}{\Delta E_{e_{kn}}}|\psi_k\rangle + |\psi_n\rangle}{\left|{\lambda_e}^2\sum_{k\neq n}\frac{|\alpha_{e_{kn}}|^2}{(\Delta E_{e_{kn}})^2} + 1\right|^2} \tag{B5}$$

and

$$|\Psi_{g_n}\rangle = \frac{\lambda_g\sum_{k\neq n}\frac{\alpha_{g_{kn}}}{\Delta E_{g_{kn}}}|\psi_k\rangle + |\psi_n\rangle}{\left|{\lambda_g}^2\sum_{k\neq n}\frac{|\alpha_{g_{kn}}|^2}{(\Delta E_{g_{kn}})^2} + 1\right|^2}. \tag{B6}$$

The probability of a like-to-like transition can now be written as

$$|\langle\Psi_{e_n}|\Psi_{g_n}\rangle|^2 = \left|\left(\frac{\lambda_e \sum_{k\neq n}\frac{\alpha_{e_{kn}}^*}{\Delta E_{e_{kn}}}\langle\psi_k| + \langle\psi_n|}{\left|\lambda_e{}^2\sum_{k\neq n}\frac{|\alpha_{e_{kn}}|^2}{(\Delta E_{e_{kn}})^2}+1\right|^2}\right)\left(\frac{\lambda_g \sum_{k\neq n}\frac{\alpha_{g_{kn}}}{\Delta E_{g_{kn}}}|\psi_k\rangle + |\psi_n\rangle}{\left|\lambda_g{}^2\sum_{k\neq n}\frac{|\alpha_{g_{kn}}|^2}{(\Delta E_{g_{kn}})^2}+1\right|^2}\right)\right|^2$$
$$= \left|\frac{\lambda_e\lambda_g\sum_{k\neq n}\frac{\alpha_{e_{kn}}^*}{\Delta E_{e_{kn}}}\frac{\alpha_{g_{kn}}}{\Delta E_{g_{kn}}}+1}{\left|\lambda_e{}^2\sum_{k\neq n}\frac{|\alpha_{e_{kn}}|^2}{(\Delta E_{e_{kn}})^2}+1\right|^2\left|\lambda_g{}^2\sum_{k\neq n}\frac{|\alpha_{g_{kn}}|^2}{(\Delta E_{g_{kn}})^2}+1\right|^2}\right|^2. \tag{B7}$$

For sites with perfect axial symmetry, the eigenstates of $\widehat{H}_Z$ are also eigenstates of $\widehat{H}_q$. Therefore, for all $k \neq n$

$$\alpha_{kn} = \langle\psi_k|\widehat{H}_q|\psi_n\rangle = 0, \tag{B8}$$

and the result of Eq. (B7) is a unity transition probability: $|\langle\Psi_{e_n}|\Psi_{g_n}\rangle|^2 = 1$.

For sites without perfect axial symmetry, the $|\psi_n\rangle$ are no longer eigenstates of $\widehat{H}_q$. As a result, the precise value of the transition probability given by Eq. (B7) is strongly dependent on the α_{kn} for the ground and excited states. The calculation of the α_{kn} requires the knowledge of the spin Hamiltonians for the ground and excited states, in which case the transition probabilities can be calculated directly, as was done for Pr^{3+}:Y_2SiO_5 in Sec. V A.

If the spin Hamiltonians for the ground and excited states are not known, the form of Eq. (B7) can be used to make a coarse approximation of the transition probability given knowledge of λ:

$$|\langle\Psi_{e_n}|\Psi_{g_n}\rangle|^2 \geqslant \left(\frac{\lambda_e\lambda_g+1}{\left(\lambda_e{}^2+1\right)^2\left(\lambda_g{}^2+1\right)^2}\right)^2. \tag{B9}$$

[1] Y. Sun, C. W. Thiel, R. L. Cone, R. W. Equall, and R. L. Hutcheson, Recent progress in developing new rare earth materials for hole burning and coherent transient applications, J. Lumin. **98**, 281 (2002).

[2] F. Könz, Y. Sun, C. W. Thiel, R. L. Cone, R. W. Equall, R. L. Hutcheson, and R. M. Macfarlane, Temperature and concentration dependence of optical dephasing, spectral-hole lifetime, and anisotropic absorption in Eu^{3+}:Y_2SiO_5, Phys. Rev. B **68**, 085109 (2003).

[3] M. Zhong, M. P. Hedges, R. L. Ahlefeldt, J. G. Bartholomew, S. E. Beavan, S. M. Wittig, J. J. Longdell, and M. J. Sellars, Optically addressable nuclear spins in a solid with a six hour coherence time, Nature (London) **517**, 177 (2015).

[4] T. W. Mossberg, Time-domain frequency-selective optical data storage, Opt. Lett. **7**, 77 (1982).

[5] W. R. Babbitt and J. A. Bell, Coherent transient continuous optical processor, Appl. Opt. **33**, 1538 (1994).

[6] P. B. Sellin, N. M. Strickland, J. L. Carlsten, and R. L. Cone, Programmable frequency reference for subkilohertz laser stabilization by use of persistent spectral hole burning, Opt. Lett. **24**, 1038 (1999).

[7] M. P. Hedges, J. J. Longdell, Y. Li, and M. J. Sellars, Efficient quantum memory for light, Nature (London) **465**, 1052 (2010).

[8] M. Gündoğan, P. M. Ledingham, K. Kutluer, M. Mazzera, and H. de Riedmatten, Solid State Spin-Wave Quantum Memory for Time-Bin Qubits, Phys. Rev. Lett. **114**, 230501 (2015).

[9] P. M. Ledingham, W. R. Naylor, and J. J. Longdell, Experimental Realization of Light with Time-Separated Correlations by Rephasing Amplified Spontaneous Emission, Phys. Rev. Lett. **109**, 093602 (2012).

[10] C. E. Wieman, D. E. Pritchard, and D. J. Wineland, Atom cooling, trapping, and quantum manipulation, Rev. Mod. Phys. **71**, S253 (1999).

[11] A. D. Cronin, J. Schmiedmayer, and D. E. Pritchard, Optics and interferometry with atoms and molecules, Rev. Mod. Phys. **81**, 1051 (2009).

[12] A. Abragam and B. Bleaney, *Electron Paramagnetic Resonance of Transition Ions* (Dover, New York, 1986), Table 20, Appendix B, pp. 874–875.

[13] R. M. Macfarlane and R. M. Shelby, Coherent transient and holeburning spectroscopy of rare earth ions in solids, in *Spectroscopy of Solids Containing Rare Earth Ions*, edited by A. A. Kaplyanskii and R. M. Macfarlane (North-Holland, Amsterdam, 1987).

[14] G. Liu, Electronic energy level structure, in *Spectroscopic Properties of Rare Earths in Optical Materials*, edited by G. Liu and B. Jacquier (Springer, Berlin, 2005).

[15] O. Guillot-Noël, P. Goldner, E. Antic-Fidancev, and J. L. Le Gouët, Analysis of magnetic interactions in rare-earth-doped crystals for quantum manipulation, Phys. Rev. B **71**, 174409 (2005).

[16] A. Louchet, J. S. Habib, V. Crozatier, I. Lorgeré, F. Goldfarb, F. Bretenaker, J.-L. Le Gouët, O. Guillot-Noël, and Ph. Goldner, Branching ratio measurement of a Λ system in Tm^{3+}:YAG under a magnetic field, Phys. Rev. B **75**, 035131 (2007).

[17] P. Goldner and O. Guillot-Noël, Magnetic interactions in Pr^{3+}:$LiYF_4$ for quantum manipulation: search for an efficient three-level Λ system, Mol. Phys. **102**, 1185 (2004).

[18] K. Holliday, M. Croci, E. Vauthey, and U. P. Wild, Spectral hole burning and holography in an Y_2SiO_5:Pr^{3+} crystal, Phys. Rev. B **47**, 14741 (1993).

[19] C. Zener, Non-adiabatic crossing of energy levels, Proc. R. Soc. A **137**, 696 (1932).

[20] G. H. Dieke, H. M. Crosswhite, and B. Dunn, Emission spectra of the doubly and triply ionized rare earths, J. Opt. Soc. Am. B **51**, 820 (1961).

[21] L. Riseberg and H. W. Moos, Multiphonon orbit-lattice relaxation of excited states of rare-earth ions in crystals, Phys. Rev. **174**, 429 (1968).

[22] M. A. Teplov, Magnetic resonance on Pr^{141} nuclei in a $Pr_2(SO_4)_3 \cdot 8H_2O$ single crystal, ZhETF, **53**, 1510 (1968) [Sov. Phys.–Usp. **26**, 872 (1968)].

[23] K. Hoffman and R. Kunze, *Linear Algebra*, 2nd ed. (Prentice-Hall, Englewood Cliffs, New Jersey, 1971), Chap. 6, p. 207.

[24] K. K. Sharma and L. E. Erickson, NMR Measurement of the Hyperfine Constant of an Excited State of an Impurity Ion in a Solid, Phys. Rev. Lett. **45**, 294 (1980).

[25] A. J. Silversmith and R. M. Macfarlane, Spectral-hole-burning study of the hyperfine interaction in axial Eu^{3+} centers in CaF_2, SrF_2, and BaF_2, Phys. Rev. B **45**, 5811 (1992).

[26] H. Goldstein, C. P. Poole, and J. L. Safko, *Classical Mechanics* (Addison Wesley, San Francisco, 2002).

[27] S. E. Beavan, M. P. Hedges, and M. J. Sellars, Demonstration of Photon-Echo Rephasing of Spontaneous Emission, Phys. Rev. Lett. **109**, 093603 (2012).

[28] D. Rieländer, K. Kutluer, P. M. Ledingham, M. Gündoğan, J. Fekete, M. Mazzera, and H. de Riedmatten, Quantum Storage of Heralded Single Photons in a Praseodymium-Doped Crystal, Phys. Rev. Lett. **112**, 040504 (2014).

[29] T. Utikal, E. Eichhammer, L. Petersen, A. Renn, S. Götzinger, and V. Sandoghdar, Spectroscopic detection and state preparation of a single praseodymium ion in a crystal, Nat. Commun. **5**, 3627 (2014).

[30] M. Lovrić, P. Glasenapp, and D. Suter, Spin Hamiltonian characterization and refinement for Pr^{3+}:$YAlO_3$ and Pr^{3+}:Y_2SiO_5, Phys. Rev. B **85**, 014429 (2012).

[31] B. B. Blinov, D. Leibfried, C. Monroe, and D. J. Wineland, Quantum computing with trapped ion hyperfine qubits, in *Experimental Aspects of Quantum Computing*, edited by H. O. Everitt (Springer, Berlin, 2005).

[32] M. Nilsson, L. Rippe, S. Kröll, R. Klieber, and D. Suter, Hole-burning techniques for isolation and study of individual hyperfine transitions in inhomogeneously broadened solids demonstrated in Pr^{3+}:Y_2SiO_5, Phys. Rev. B **70**, 214116 (2004).

[33] R. Kolesov, K. Xia, R. Reuter, R. Stöhr, A. Zappe, J. Meijer, P. R. Hemmer, and J. Wrachtrup, Optical detection of a single rare-earth ion in a crystal, Nat. Commun. **3**, 1029 (2012).

[34] I. Nakamura, T. Yoshihiro, H. Inagawa, S. Fujiyoshi, and M. Matsushita, Spectroscopy of single Pr^{3+} ion in LaF_3 crystal at 1.5 K, Sci. Rep. **4**, 7364 (2014).

[35] N. Ohlsson, R. K. Mohan, and S. Kröll, Quantum computer hardware based on rare-earth-ion-doped inorganic crystals, Opt. Commun. **201**, 71 (2002).

[36] J. J. Longdell, Quantum Information Processing in Rare Earth Ion Doped Insulators, Ph.D. thesis, Australian National University, 2003.

[37] M. Afzelius, I. Usmani, A. Amari, B. Lauritzen, A. Walther, C. Simon, N. Sangouard, J. Minář, H. de Riedmatten, N. Gisin, and S. Kröll, Demonstration of Atomic Frequency Comb Memory for Light with Spin-Wave Storage, Phys. Rev. Lett. **104**, 040503 (2010).

[38] B. Lauritzen, S. R. Hastings-Simon, H. de Riedmatten, M. Afzelius, and N. Gisin, State preparation by optical pumping in erbium-doped solids using stimulated emission and spin mixing, Phys. Rev. A **78**, 043402 (2008).

[39] M. Afzelius, M. U. Staudt, H. de Riedmatten, N. Gisin, O. Guillot-Noël, P. Goldner, R. Marino, P. Porcher, E. Cavalli, and M. Bettinelli, Efficient optical pumping of Zeeman spin levels in Nd^{3+}:YVO_4, J. Lumin. **130**, 1566 (2010).

[40] E. Fraval, M. J. Sellars, and J. J. Longdell, Method of Extending Hyperfine Coherence Times in Pr^{3+}:Y_2SiO_5, Phys. Rev. Lett. **92**, 077601 (2004).